Computers and Chemical Engineering 34 (2010) 1058–1071

Contents lists available at ScienceDirect

Computers and Chemical Engineering

journal homepage: www.elsevier.com/locate/compchemeng

Understanding variation in roller compaction through finite element-based process modeling

John C. Cunningham [a,b,*], Denita Winstead [b], Antonios Zavaliangos [a]

[a] Department of Materials Science and Engineering, Drexel University, Philadelphia, PA, United States
[b] Johnson & Johnson Pharmaceutical R&D, Spring House, PA, United States

ARTICLE INFO

Article history:
Received 11 September 2009
Received in revised form 5 April 2010
Accepted 6 April 2010
Available online 14 April 2010

Keywords:
Roller compaction
Process modeling
Finite element
Dry granulation

ABSTRACT

One of primary goals of the Quality by Design initiative in the pharmaceutical industry is to reduce variation in the product quality through increased understanding and control of the manufacturing process. In the case of roller compaction, in which mixtures of active and inert powders are fed via a screw to counter-rotating rolls, drawn into the nip region and compacted under hydrostatic and shear stresses, variation in density of the roller compacted material has been commonly observed. In the experimental part of this work we report measurements of pressure and shear under the rolls which show variation of the local stress conditions along the width of the roll which evolves with time. Also roll pressure and shear stress appear to persist past the minimum roll separation. To further investigate the potential causes of these variations, 2D and 3D explicit finite element-based models with adaptive meshing and arbitrary Eulerian–Lagrangian capabilities were developed. A Drucker-Prager/cap constitutive model was used to describe the mechanical behavior of the powder. Microcrystalline cellulose was used as the model powder. The 2D model was used to evaluate the effects of feed stress, roll friction on roll force, profiles of roll pressure and roll shear stress, nip angle and relative density of the compacted powder. The results indicated increasing feed stress, and/or increasing roll friction lead to higher maximum roll surface pressure and attendant relative density at the exit. The results may be explained by the location of the nip angle and the amount of pre-densification in the feed zone. Simulations with pressure-dependent frictional coefficients indicated significant differences in densification. In addition, oscillating feed stress conditions revealed periodic variations in roll pressures and relative densities. The 3D model predicted lower roll pressure and densities near the edges due to presence of side seal friction. Variable inflow of material along the roll width was related to variation in roll pressure. Overall, the model predictions followed experimental trends. The process modeling provided greater insight into the potential causes of the variation in density of the roller compacted material and highlighted the significance of the design of the feed system, which may be used to evaluate potential design improvements.

1. Introduction

Roller compaction is a unit operation in the dry granulation process, a commonly used pressure-induced agglomeration technique in the pharmaceutical industry in which granules with acceptable flowability, compaction, compositional uniformity, and chemical stability are formed from feed material consisting of mixtures of active and excipient (inert) powders. During the dry granulation process the dry powders of the active ingredient and excipients, e.g., dry binders, disintegrants, diluents and lubricants, are mixed in a blender. The powder mixtures are then roller compacted and milled to form granules. The resulting granulation is typically blended with a lubricant and either encapsulated or compressed into a tablet.

During roller compaction, the powder mixture is continuously fed – often with the assistance of a screw or auger feeder – to two counter-rotating rolls, which draw and compact the powder between the rolls into strips or flakes of compacted material. The feed powder is densified by a combination of shear and hydrostatic stresses that develop from the feed stress, friction at the rolls and the confining boundaries of rolls, screw and lateral side seals.

While roller compaction is often used successfully within the pharmaceutical industry at the production scale, engineers and scientists frequently rely on an empirical approach to define and optimize the formulation and process. The use of statistical design of experiments (Herting & Kleinebudde, 2007; Weyenberg, Vermeire, Vandervoort, Remon, & Ludwig, 2005) or neural networks (e.g., Mansa, Bridson, Greenwood, Barker, & Seville, 2008), can yield valuable information, but they are generally limited

* Corresponding author at: Department of Materials Science and Engineering, Drexel University, Philadelphia, PA, United States.
E-mail address: azavalia@coe.drexel.edu (J.C. Cunningham).

0098-1354/$ – see front matter © 2010 Elsevier Ltd. All rights reserved.
doi:10.1016/j.compchemeng.2010.04.008

to the particular material and roller compactor evaluated. There are a number of reasons for this high reliance on the empirical approach: (1) lack of experimental measurements of important process parameters and (2) limited effort on process modeling, which is due to complexities in both physical process geometry and mechanical behavior of compacting powders. During the process, important process conditions, e.g., surface roll pressure or feed stresses, are typically not measured due to the cost and difficulty in the design and implementation of such measurement systems. These parameters are, however, essential to the understanding and control of the feeding of the powders to the roll and to the development of the compact properties, e.g., the density of the compact is directly correlated to the maximum roll pressure developed. Without measurement of these parameters, researchers must depend on such indirect measurements as the overall roll force. In addition to the lack of detailed process measurements, there has been limited process modeling to date. Process modeling, however, when coupled with experimental studies, can provide a rational scientific framework to: (i) probe the underlying physical processes; (ii) understand relative importance of various material, equipment and process factors; and (iii) predict and optimize formulations and process parameters. While roller compaction appears be a simple operation, it is a complex deformation process involving highly non-linear contact and material behavior with complicated boundary conditions, e.g., oscillating screw feeding in the feed zone. Finally, the feed powder undergoes significant evolution in mechanical properties from its rather loose state in feed zone to the compacted ribbon or flake upon exit of the rolls. Capturing of these changes requires an appropriately calibrated constitutive model to be implemented into a process model.

The overall goal of this research is to provide greater understanding of the sources of variation in roller compaction process through a series of experimental studies and modeling efforts. Specific objectives include:

- Understand roller compaction through detailed experimental studies on model pharmaceutical powders using an instrumented roller compactor capable of measuring the feed force induced by a screw feeder and the roll surface pressure and roll shear stress at different locations across the roll width.
- Develop process models for the roller compaction process and conduct parametric studies to (1) understand the relative importance of the roller compaction parameters, e.g., powder/roll friction, entry angle, and feed stress and (2) predict the development of contact stresses, i.e., roll pressure and roll shear stress, internal stress and strain fields, densification, and loading conditions, e.g., roll force and roll torque.

Special emphasis is placed on the understanding potential sources of variation in the roller compaction process that lead to variation in resulting properties of the roller compacted material, e.g., relative density of compacted ribbon.

2. Background

A schematic of the regions of compaction is provided in Fig. 1. Four angles, the entry angle, α_{entry}, the nip angle, α_{nip}, the neutral angle, $\alpha_{neutral}$ and the release angle, $\alpha_{release}$, also shown in Fig. 1, demarcate the various regions. The feed material is delivered to the rolls under gravity or by a force or screw feeder. Under gravity feed, adjustable tongues may control the flow of powder with the distribution across the roll width achieved by rotating devices mounted above the rolls. The screw feeder induces a positive feed pressure to be applied and can be used as part of a control system. The end of the feeding zone is traditionally defined by the entry angle, α_{entry}

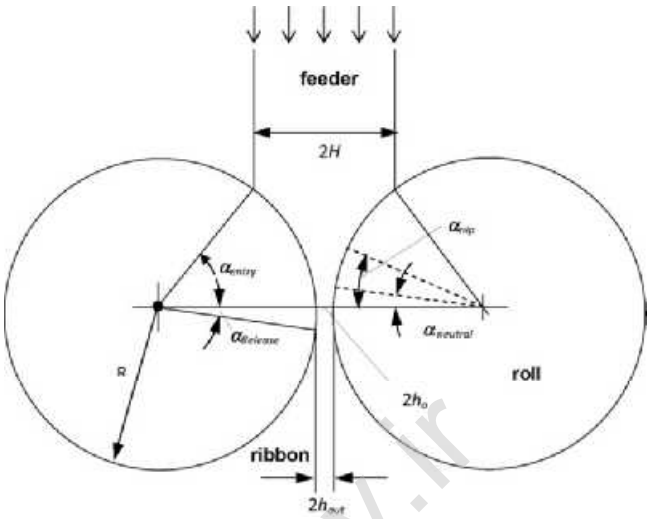

Fig. 1. Schematic of regions of roller compaction. Basic geometric parameters are defined. Four angles are marked: (a) entry angle, α_{entry}, (b) nip angle, α_{nip} (at the transition from slipping to being gripped by the rolls), (c) neutral angle, $\alpha_{neutral}$ (where the shear stress on the roll surface changes sign) and (d) release $\alpha_{release}$ (where the ribbon leaves the rolls).

(see Fig. 1) which marks the point where the powder comes into contact with the rolls. The area where the powder is in contact with the rolls is divided in the slip zone ($\alpha_{entry} > \alpha > \alpha_{nip}$) and the compaction or nip (stick) zone ($\alpha > \alpha_{nip}$) (Pietsch, 1987). Within the slip zone, the feed pressure and the friction forces at the roll/powder interface drive the powder toward the roll gap region. The stresses developed are relatively low. The peripheral speed of the rolls is higher than the speed of the material adjacent to the rolls in this region. The material is thus experiencing slipping at the roll surface.

For $\alpha < \alpha_{nip}$, the powder is sticks to the rolls and follows the peripheral speed of the rolls. The stress begins to rise rapidly and the material undergoes greater densification than in the slip zone. This densification is accomplished by plastic deformation and/or fracture of the particles. The roll pressure rapidly increases to a maximum in the nip region. At the neutral angle, $\alpha_{neutral}$, the direction of the friction force on the roll reverses direction, i.e., for $\alpha > \alpha_{neutral}$ frictional forces push the powder towards the gap, while for $\alpha < \alpha_{neutral}$ the frictional forces are directed away from the gap. After the roll pressure reaches its maximum, it begins to drop as the compacted powder progresses through the roll gap and is finally released at angle $\alpha_{release}$. A third zone may be present, the extrusion zone, close to the release angle. In this zone, the compacted material moves faster than the peripheral speed of the rolls, i.e. there is a transition from sticking in the compaction zone back to slipping.

To guide the process modeling effort, experimental studies using an instrumented roll capable of measuring both normal roll pressure and roll shear stress were conducted. There have been a number of important experimental contributions by researchers in fields outside the pharmaceutical industry—namely the metals, mineral and chemical industries. For example, the earliest measurements of the contact stresses on the roll were reported for metal powders (Chekmarev, Klimenko, & Vinogradov, 1963; Katashinskii & Vinogradov, 1965). Similar measurements were made for mineral and chemicals (Andersen, 1990; Dec & Komarek, 1991; Lecompte et al., 2005; Lubjuhn, Sander, & Schonert, 1994; Schonert & Sander, 2002). More recently, roll surface pressure measurements have been made for pharmaceutical powders (Bindhumadhavan, Seville, Adams, Greenwood, & Fitzpatrick, 2005; Simon & Guigon, 2000; Simon & Guigon, 2003; Zega, Cunningham, Roland, Katdare, & Reynolds, 1998). In addi-

tion to the evolution of the contact stresses developed for various roller compactors and materials, experimental studies focusing on variation induced by the roller compactor design, e.g., feed system, were conducted using a variety of approaches and techniques: a specialized feed system instrumented with load cells and pressure gauges (Dec & Komarek, 1993) and color change using tracers (Funakoshi, Asogawa, & Satake, 1977), transmitted light (Guigon and Simon, 2003; Simon & Guigon, 2003), photomicroscopy (Tunderman & Singer, 1969), micro-indentation (Freitag, Reincke, Runge, Grellmann, & Kleinbudde, 2004; Miguelez-Moran, Wu, Dong, & Seville, 2009), X-ray tomography (Miguelez-Moran et al., 2009), and near infrared (NIR) spectroscopy (Bijlani, Anderson, Adeyeye, & Drennen, 2003; Gupta, Peck, Miller, & Morris, 2004) on the roller compacted strips. These studies highlighted the relatively complex interrelationship between powder properties, equipment design and processing parameters and resulting compacted material properties. To further understand these relationships, modeling of roller compaction has also been conducted.

Over the past four decades, there have been several efforts to model roller compaction of powder (Dec & Komarek, 1991; Gun, Stebunov, & Katashinskii, 1986; Johanson, 1965; Johanson, 1973; Katashinskii, 1966; Katashinskii & Shtern, 1983a; Katashinskii & Shtern, 1983b; Musikhin, 1977; Shima & Yamada, 1984). A review of these various modeling efforts was recently published (Dec, Zavaliangos, & Cunningham, 2003). Modeling of roller compaction has been challenging due to a number of reasons including: (i) the non-linear behaviors related to the contact or frictional conditions at the roll surface and to the constitutive behavior of the deforming powder which undergoes significant evolution of its mechanical properties as it is densified; (ii) the lack of material-related experimental inputs measured under relevant process conditions, e.g., frictional coefficient of roll/powder under stress states encountered during roller compaction; and (iii) experimental difficulties of evaluating the actual process including the boundary conditions, e.g., feed stress and friction, and initial conditions, e.g., density of the powder in the feed zone; despite these challenges, the development of simplified process models can provide important valuable insight into roller compaction. To overcome these challenges, finite element-based modeling has been increasingly applied to study the compaction of pharmaceutical powders—for example, in die compaction or tableting (Alkhattat & Alhassani, 1987; Han et al., 2008; Michrafy, Ringenbacher, & Tchoreloff, 2002; Sinka, Cunningham, & Zavaliangos, 2003; Sinka, Cunningham, & Zavaliangos, 2004; Wu et al., 2005), diametrical compression testing of tablets (Procopio, Zavaliangos, & Cunningham, 2003) and roller compaction (Cunningham & Zavaliangos, 2002). The present process modeling also uses the finite element approach to model roller compaction.

3. Experimental

3.1. Materials

The materials used in the experimental runs included: microcrystalline cellulose (MCC: Avicel PH102, FMC) and magnesium stearate (Mallinckrodt). Mixtures of these powders were prepared by blending in a V-shaped tumble blender (Patterson-Kelley). Blending time for the mixtures was 5–15 min.

3.2. Roller compaction

A instrumented roller compactor (RC100, Roland Research Devices, Inc., Trenton, NJ) was used in this study. This roller compactor had a floating roll design with roll diameter of 100 mm width of 35 mm. The surface of the rolls was textured. The powder was fed into the rolls by a vertical screw. Screw speed and feed force, roll speed, roll force, roll torque and roll gap were measured during a run. A versatile control system was implemented that was capable of running under single loop control for screw speed, roll speed, and roll force roller or with feedback control loops, e.g., constant roll gap or constant feed force control with the error feeding back to screw motor. The roll was instrumented with embedded load cells that measure the contact stresses. The load cells have a rectangular design, which was capable of measuring approximately 0.7° of angular position, was based on an instrumented roll by (Schonert & Sander, 2002) that enabled measurement of both normal and shear stresses at the roll (Fig. 2). The drive system for the rolls allowed variable rotational speeds between 0 and 10 rpm. Additional details on these experiments can be found in (Cunningham, 2005).

An example run (roll force = 27.5 kN, roll speed = 4 rpm, feed screw speed = 12.7 rpm, feed screw force of 52.6 N, roll gap = 1.20 mm for MCC with 0.50% magnesium stearate) is discussed in detail. The profiles of roll pressure and roll shear stresses as a function of position along the roll width is provided in Fig. 3. Several notable observations can be made upon examination of these profiles:

- The roll pressure slowly begins to rise at approximately 10° and reach a maximum close to 0° before rapidly returning to zero between 5 and 8° on the exit side. Note that the sampling rate and roll speed resulted in measurements every 1° thus it is difficult to isolate the exact position of the maximum. In the case of smooth roll design the maximum occurred prior to the centerline of the rolls at 1° (Cunningham, 2005; Zega et al., 1998).
- There is significant variation in maximum roll pressure along the roll width. In this example the overall maximum roll pressure is off center (position C in the inset of Fig. 3). The position varies with time across the gap, i.e., upon successive rotations of the rolls.
- The roll shear stresses gradually build on the entry side of the rolls with local maximum values of 14–24 MPa. The shear stress then reduces to zero at the neutral angle and proceeds to reverse direction and build rapidly to very high values of 28–100 MPa on the exit side of the rolls at approximately 2°. The neutral angle ranges from 0 to 1.2°.
- The persistence of the pressure and shear stresses at the exit of the roll is rather unexpected but is consistent with the measurements of (Schonert & Sander, 2002) on quartz powder.

The profiles of roll pressure, p_r, and roll shear stress, t_r, were used to calculate the corresponding roll force using the following equation:

$$F = \int [(p_r \cos\alpha) + (t_r \sin\alpha)]\, dA \quad (1)$$

where α is the angular position under the rolls and dA is the differential area on which roll pressure and roll shear are applied ($dA = RW\, d\alpha$, where R is the roll radius, W is the roll width and $d\alpha$ is the differential angle shown in Fig. 3b). Using the experimentally obtained values of p_r (α,z) and t_r (α,z), the roll force was calculated to be 26.5 kN compared to the measured value of 27.4 kN, thus within 4% of the measured value and helps validate the design of the pressure/shear stress sensor. The relative contribution of the roll shear stress is only 3% so that assumption that the roll pressure contributed primarily to the roll force is valid for this geometry.

Contour plots of the roll pressure with respect to the roll width and rolling direction for five successive revolutions are shown in Fig. 4. The location of overall maximum roll pressure varied from across the roll width on both sides of the center (0 mm). The movement of the overall maximum roll pressure is related to the rotating

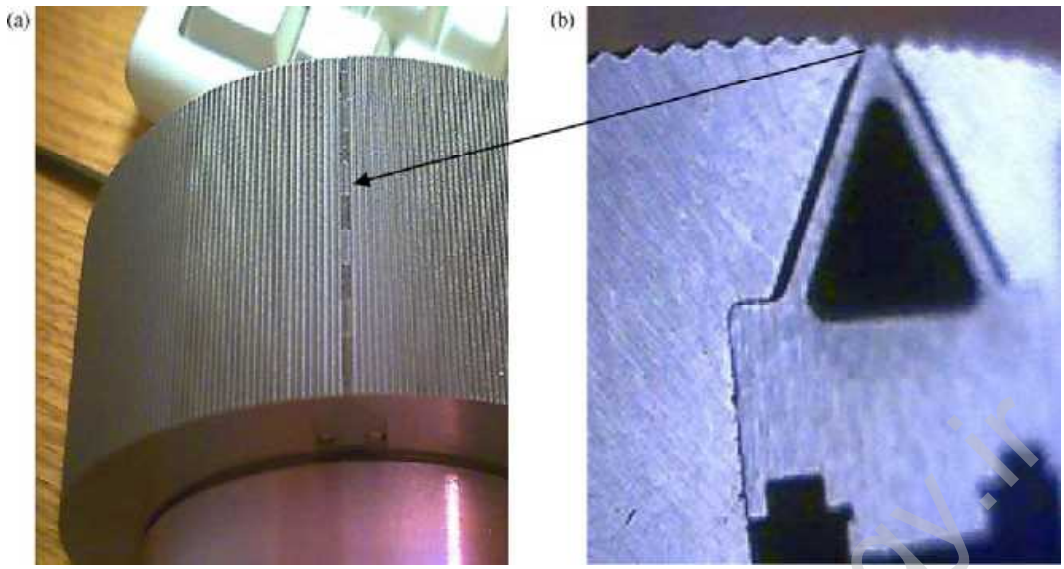

Fig. 2. (a) Side view of instrumented roll with roll load. (b) View of textured roll surface with five load cells across the roll.

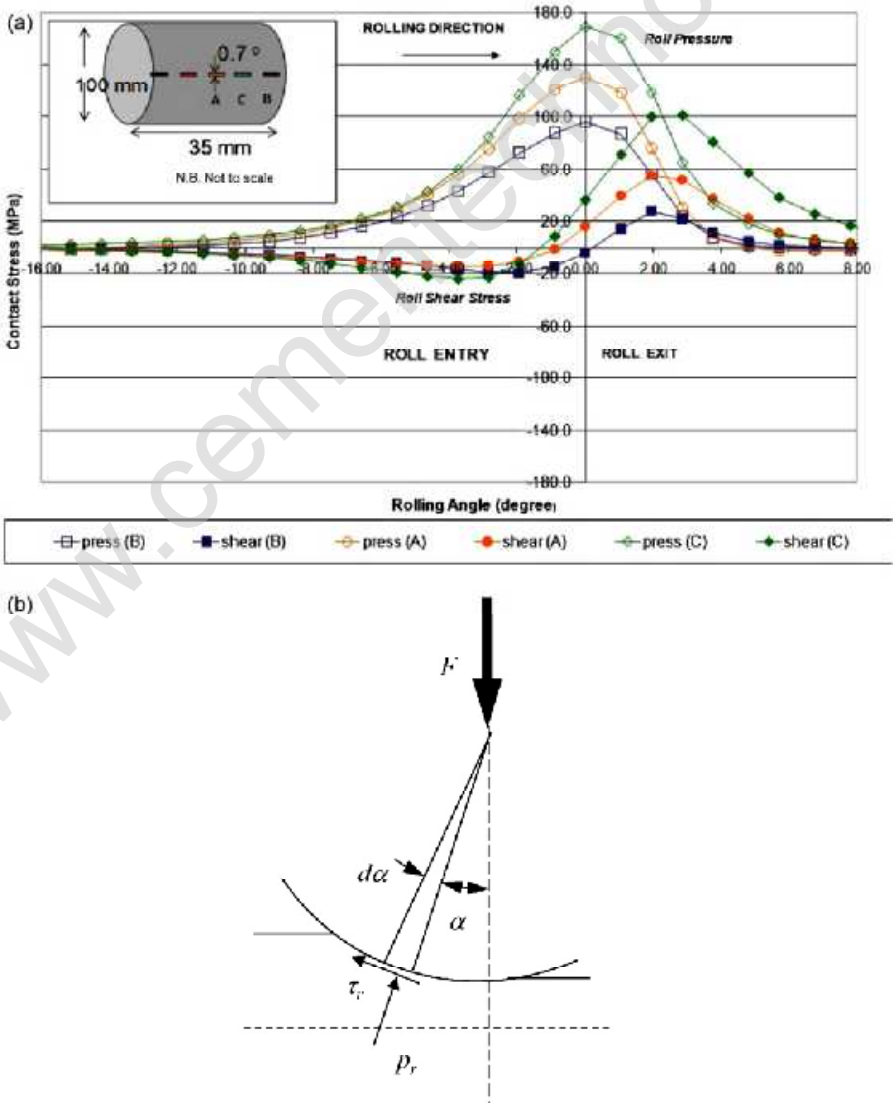

Fig. 3. (a) Profiles of roll pressure and roll shear stress for various locations across the roll width, (b) equilibrium diagram for the calculation of roll force.

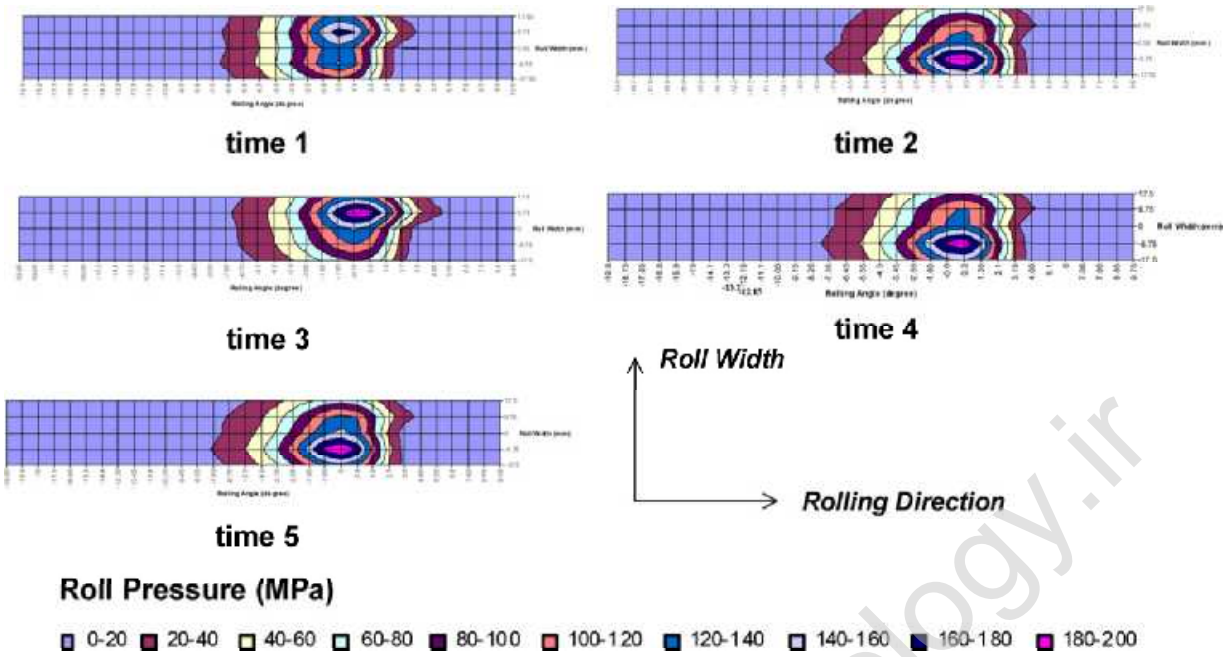

Fig. 4. Contours of roll pressure with respect to rolling directions and roll width. The middle of the roll along its width is designation of 0 mm. Time 1–5 represent five successive revolutions.

nature of the screw feeder. The screw is placed in the center of the roll gap but its pushing action is not symmetric around its axis of rotation because of the helical geometry. The rotation of the screw introduces a pushing action with a peak that oscillates along the gap width. The sampling rate and the position of the sensors translate the oscillatory nature of the variation of pressure into the pattern shown in Fig. 4. In addition, the frictional resistance at the side seal further reduces the flow to the edges. These geometrical and boundary effects along with the mechanical behavior of low density powders create a complex, non-homogeneous distribution of powder in the feed zone. These feed effects as also observed by several researchers, e.g. (Dec & Komarek, 1993; Guigon and Simon, 2003; Miguelez-Moran et al., 2009; Simon & Guigon, 2003) can directly manifest themselves in the local roll pressure profiles developed and the local density distribution of the resulting compact. In order to probe the causes of these observed variations, the modeling of roller compaction in 2- and 3-dimensions using the finite element approaches was undertaken.

4. Two-dimensional finite element model

The complex geometry and contact conditions, and the mechanical behavior of the powder necessitate the use of the finite element method to solve the equations of continuity and equilibrium. The mechanical behavior of the rolled powder was modeled by the Drucker-Prager/cap model (DP/C). This is an attractive model for compaction analysis because it combines adequate detail of the mechanical performance of compacted powders and reasonable experimental calibration requirements. The details of this model were described extensively in our previous papers (Cunningham, Sinka, & Zavaliangos, 2004; Dec et al., 2003; Sinka et al., 2003; Sinka et al., 2004; Zavaliangos, Galen, Cunningham, & Winstead, 2008). A brief description is presented here for completeness. The heart of the model is the yield locus that demarcates stress conditions that cause the compact to deform reversibly (elastically) and irreversibly (plastically) for a particular level of out of die relative density, RD. This demarcation, consists of: (a) a Mohr–Coulomb shear failure line which describes the behavior of the powder under low hydrostatic pressure, i.e., high shear, conditions and (b) a cap surface which describes the powder densification under high hydrostatic pressure. The two parts of the yield locus $F(p,q,RD) = 0$, are defined as a function of hydrostatic pressure, p, and equivalent Mises stress, q, which in turn are defined in terms of the components of the stress tensor σ_{ij} as:

$$p = -\frac{1}{3}(\sigma_{11} + \sigma_{22} + \sigma_{33}), \tag{2}$$

and

$$q = \sqrt{\frac{3}{2}((\sigma_{11} + p)^2 + (\sigma_{22} + p)^2 + (\sigma_{33} + p)^2 + 2\sigma_{12}^2 + 2\sigma_{23}^2 + 2\sigma_{13}^2} \tag{3}$$

The shear failure line uses two material parameters, the cohesion d and the internal friction angle β, while the cap surface is an ellipse centered at $(pa, 0)$ in the p–q plane and has an eccentricity of R. A simplified version of the model is used here with cohesion, internal friction angle and eccentricity to be constant at 0 MPa, 65°, and 0.6, respectively. Linear elastic behavior is assumed with a Young's modulus of 5 GPa and a Poisson's ratio of 0.25. It should be noted that theses material parameters are known to evolve as the material densifies, i.e., are a function of the relative density (e.g., Cunningham et al., 2004), however, for the initial modeling effort, they are assumed constant. The introduction of the relative density-dependent material parameters will require the development of a user-defined constitutive model, i.e., VUMAT in ABAQUS (Hibbitt, Karlsson, & Sorensen, 2001).

The model is completed by a plastic flow potential, $G(p,q,RD)$, which relates the plastic strain increment with the local stresses:

$$d\varepsilon_{ij}^{pl} = d\lambda \frac{\partial G(p,q)}{\partial \sigma_{ij}} \tag{4}$$

The plastic potential G, coincides with the yield locus in the region of the cap (associated flow rule). Its form in the region of the shear failure line is an ellipse that starts at the intersection of the failure line with the p-axis and joins the cap at the corner of the yield locus. The relative density evolves based on the trace of the

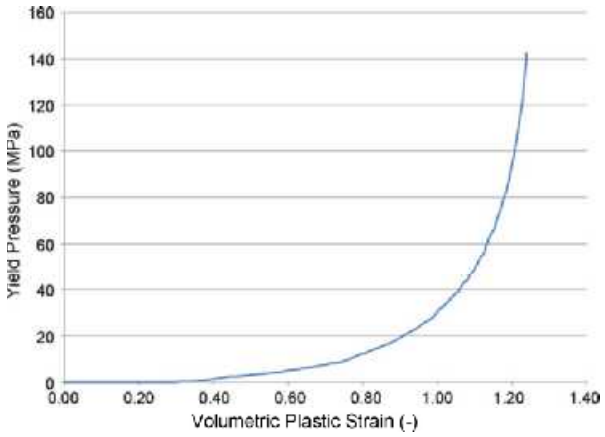

Fig. 5. The volumetric plastic strain versus yield pressure for microcrystalline cellulose with 1 wt% magnesium stearate.

plastic strain increment tensor:

$$d(RD) = -RD\sum_{t=1}^{3} d\varepsilon_{ii}^{pl} = -RD\ d\lambda \frac{\partial G(p,q)}{\partial p} \quad (5)$$

The hardening characteristics of microcrystalline cellulose with 1 wt% magnesium stearate are defined by the volumetric plastic strain versus yield pressure as shown in Fig. 5. In all simulations the initial relative density of the material was taken to be $RD_0 = 27\%$.

The constitutive model summarized above, was implemented in an arbitrary Lagrangian Eulerian finite element framework with adaptive meshing. The use of the finite element analysis will provide further insight into the stress and displacement fields during roller compaction without the need for ignoring the through-the-thickness variation that limits the earlier slab analysis (e.g., Dec & Komarek, 1991; Johanson, 1965).

Plane strain conditions are assumed for the 2D FEM analysis which in addition to zero out of plan strain it implies that is that there is no variation of the deformation field in the transverse to the rolling direction. To keep the analysis tractable the following approximations are made:

- The effect of interstitial air is ignored.
- The deformation of the rolls due to the roll pressure is ignored.
- Coulomb friction is assumed on the powder/roll interface.
- Gravity and inertia are omitted.
- The effect of the screw feeder is approximated by a uniform or oscillatory stress at the entry angle.

Because the conditions before the nip angle are such that significant shearing is expected, a modified DP/C model was chosen (Cunningham et al., 2004). This model takes into account the weak response of compacted powders in shearing and is readily available in commercial finite element programs such as ABAQUS, which was used here.

To address the issues associated the mesh distortion in the roller compaction problem, the arbitrary Lagrangian–Eulerian (ALE) and adaptive mesh capabilities within ABAQUS/Explicit were used. To avoid restricted stability condition and integration inaccuracies from distorted elements, a re-meshing algorithm was employed (Hibbitt et al., 2001). In the analysis of this process, the steady state condition is of primary interest. Based on these considerations, it is natural to consider the influx of powder to flow through an Eulerian inflow boundary as depicted in Fig. 6. Similarly on the exit side, an Eulerian outflow is defined. The material mesh represents a control volume in which material enters and exits. At the Eulerian inflow, the powder with a pre-defined initial relative density, flows in the rolling direction into the mesh domain. The default settings for remeshing were used, e.g., a single mesh sweep per increment with volumetric smoothing in which nodes are relocated by computing a volume-weighted average of the element centers in the elements surrounding the node (Hibbitt et al., 2001). The powder is subjected to an evenly distributed load applied in the rolling direction, along the thickness direction. This stress represents the feed stress induced by the feed system. Based on the symmetry, only the top half of the material mesh is analyzed. In the feed zone material mesh is constrained by the feeder boundary, which is defined using rigid elements. To simplify the analysis, the contact at the interface between the feeder and powder is assumed to be frictionless.

The 100 mm diameter roll is modeled as a rigid body in all simulations. The roll gap was kept constant to $2h_0 = 2$ mm for all runs. The roll/powder was modeled as Lagrangian boundary with the contact defined as a kinematic contact formulation (Hibbitt et al., 2001). Two-dimensional plane strain with reduced integration elements (CPE4R) was employed to construct the mesh. To assess the optimal mesh density for the deformable mesh, a series of simulations with varying mesh densities was conducted. Based on the optimal combination of accuracy, resolution and computational time, the 70×12 mesh was used in the simulations. To identify when the roller compaction simulation reaches steady state, the simulation is allowed to proceed until the roll force, F_{roll}, and roll torque, T_{roll}, reach relatively constant values.

4.1. Variation in through-the-thickness dimension

An example of the 2D analysis ($\alpha_{entry} = 20.5^\circ$, feed stress, $\sigma_o = 0.025$ MPa, and friction coefficient, $\mu_{roll} = 0.4$) is used to examine the roller compaction process in detail. The resulting roll pressure and shear stress are shown in Fig. 7. The shape of the roll pressure curve is similar to the experimental pressure profile. The peak pressure is also observed to be just before the minimum separation of the rolls (at an angle of $\sim 0.6^\circ$ from the minimum gap). Similar analysis for a smooth roll design (Cunningham, 2005; Zega et al., 1998) also placed the peak pressure located before the minimum separation of the gap. Note that the maximum relative density of the strip, RD_{max} is achieved at the centerline. Therefore, the location of peak pressure and maximum relative density do not coincide, which is contrary to common claims (e.g., Pietsch, 1987). A gradual increase of the roll pressure in the entry region and rapid unloading that extends the stressed region beyond the minimum roll separation is observed. The neutral angle does not coincide with the maximum pressure angle. In fact, it occurs just before (approximately 0.5°) the peak roll pressure. This result is also supported by experiments of others (Schonert & Sander, 2002).

The identification of the slip and stick (nip) regions can be easily performed by comparing the local speed of the mesh in contact with the roll against the roll speed. Recall also that the friction model implemented in ABAQUS dictates that slipping occurs when the shear stress, τ_r and the surface pressure, p_r are related by the Coulomb law, $t_r = \mu_{roll} p_r$. Fig. 8 shows clearly:

(a) a slipping region close to the entry angle where the powder moves slower than the roll;
(b) a region where the powder sticks to the roll since $t_r < \mu_{roll} p_r$; and
(c) a second slip region at the exit of the rolls where the powder moves faster than the roll in an extrusion-like fashion.

The forward slip is common when the powder is densified to high relative densities. A fully dense material, when rolled, slips everywhere in the rolling region except at the neutral angle. Therefore, the presence of the forward slipping region close to the roll exit is not unexpected, but is a subject that has not been discussed

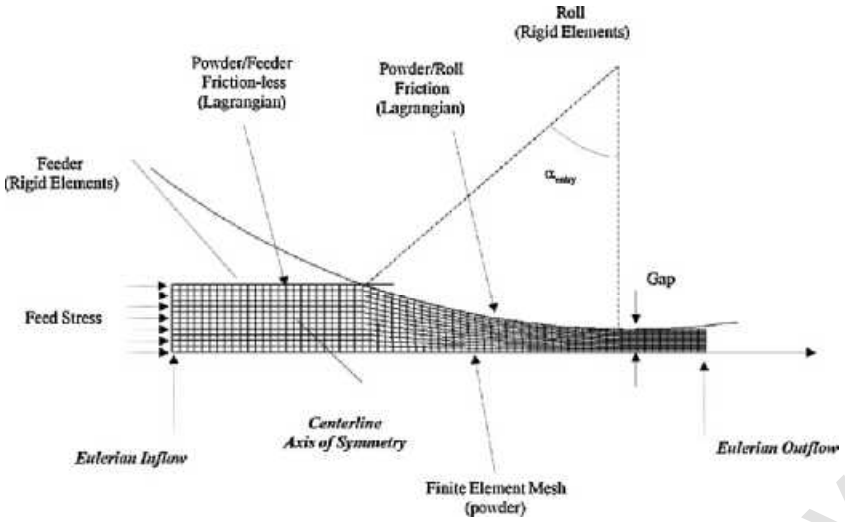

Fig. 6. Schematic of finite element mesh for roller compaction with notation of axis of symmetry, Eulerian inflow and outflow, Lagrangian roll and feeder boundaries and rigid bodies for the roll and feeder.

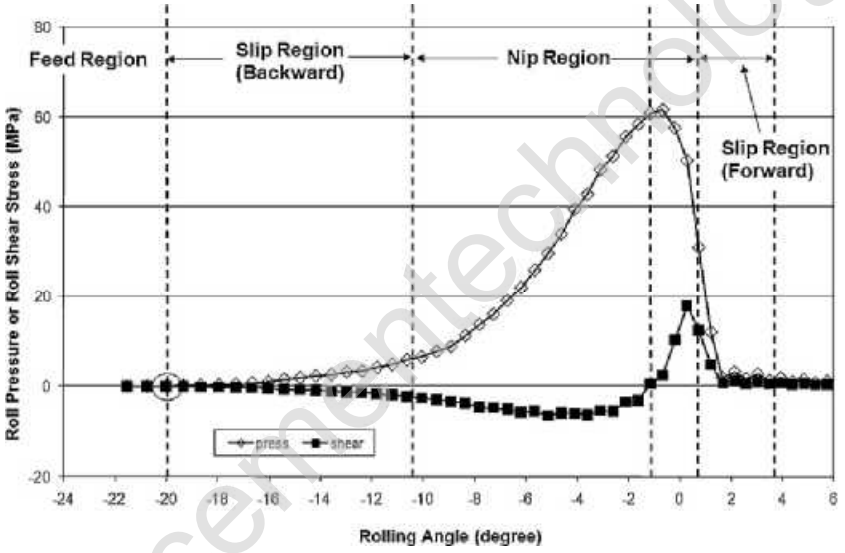

Fig. 7. The roll pressure and roll shear stress versus rolling angle for example simulation ($\alpha_{entry} = 20.5°$; $\sigma_o = 0.025$ MPa; $\mu_{roll} = 0.4$).

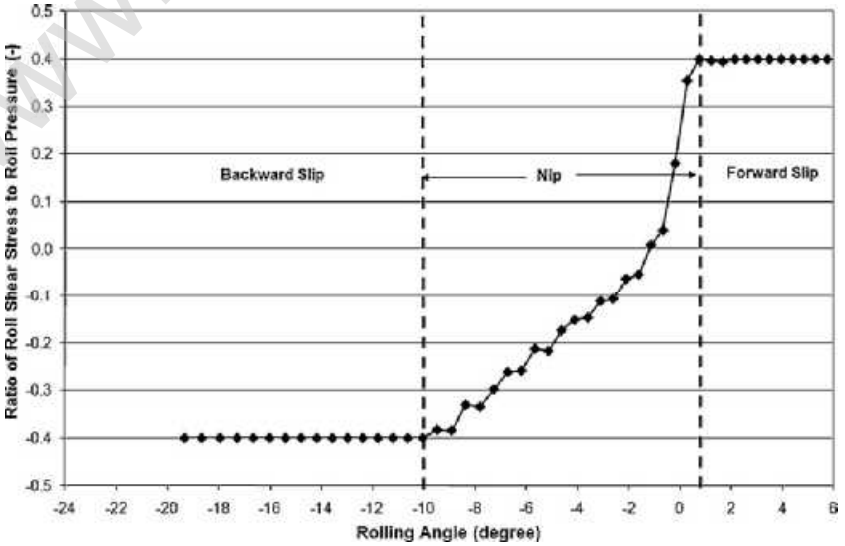

Fig. 8. The ratio of roll shear stress to roll pressure for example simulation ($\alpha_{entry} = 20.5°$; $\sigma_o = 0.025$ MPa; $\mu_{roll} = 0.4$).

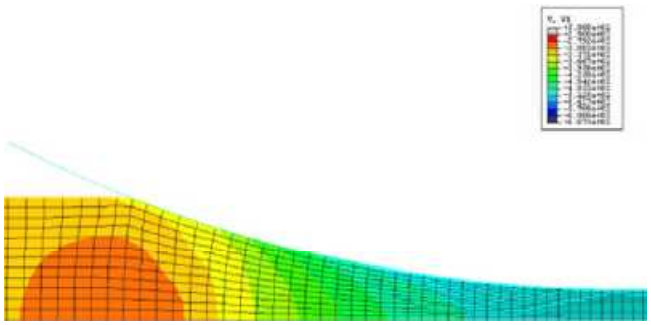

Fig. 9. Contours of velocity in the rolling direction in mm/s ($\alpha_{entry} = 20.5°$; $\sigma_o = 0.025$ MPa; $\mu_{roll} = 0.4$).

in the literature. It is also notable that the peak of shear stresses after the neutral angle is about three times the corresponding peak before the neutral angle, which is in general agreement with our experimental measurement. Although the roller compaction of pharmaceutical powders typically operates at very small roll gap to diameter ratios, which should promote minimal through-the-thickness variation at least close to the exit, there may, however, be significant through-the-thickness variation closer to the entry angle. Fig. 9 shows that there is significant variation of the velocity in the rolling direction close to the entry angle. The velocity at $\alpha = \alpha_{entry}$ is 20% smaller at the center than close to the roll. The velocity becomes more uniform downstream but it is evident that the through-the-thickness inhomogeneity from the early stage may persist as the powder is compacted further. In addition, the shear stress and strain reversed direction in the rolling direction. Given compacted pharmaceutical powders are generally weak under shear, these variations in shear may contribute to properties of the resulting compact, e.g., fracture and lamination.

Table 1
Effect of roll friction coefficient on nip angle, maximum roll pressure and relative density at exit.

Roll friction coefficient	Nip angle (°)	Maximum roll pressure (MPa)	Relative density at exit
0.30	7.0	35	0.71
0.35	8.2	50	0.78
0.40	10.0	75	0.81
0.50	13.5	130	0.89
0.60	14.5	210	0.91

4.2. Effect of roll friction

As observed in Table 1, the nip angle, maximum roll pressure and maximum relative density increase as the coefficient of roll/powder friction increases. The powder is gripped sooner by

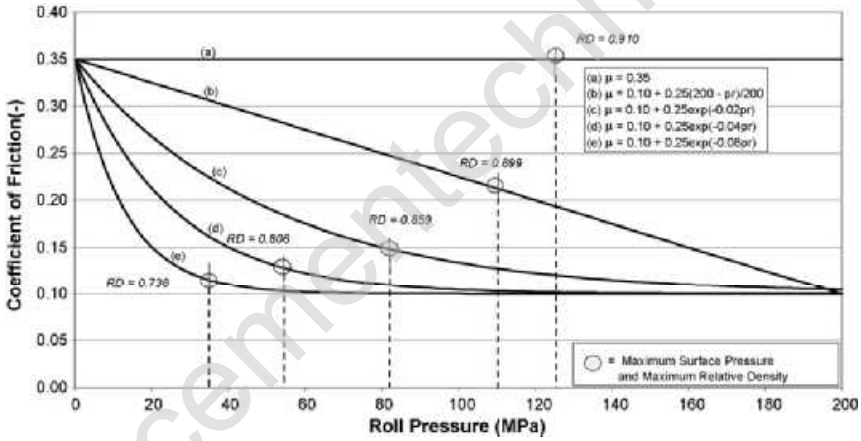

Fig. 10. Maximum roll pressure and maximum relative density as function varying definition of roll/powder friction ($\alpha_{entry} = 20.5°$; $\sigma_o = 0.400$ MPa).

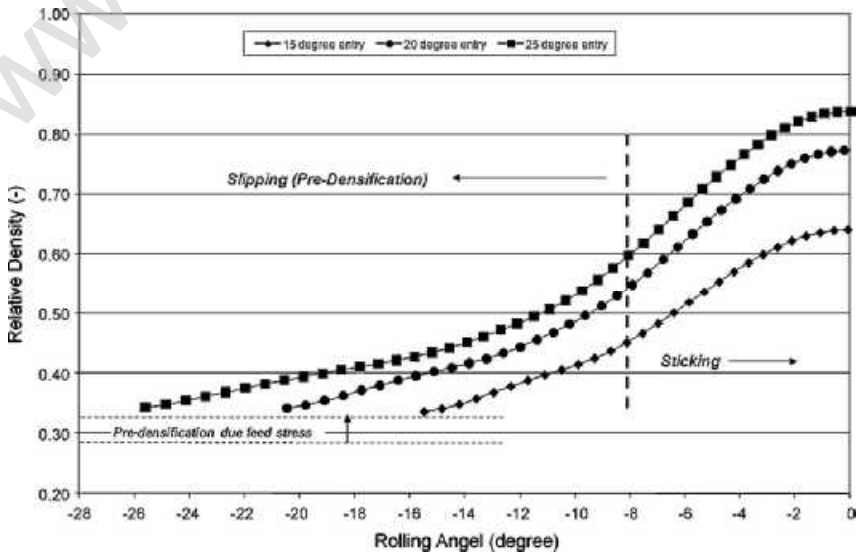

Fig. 11. Evolution of relative as function of rolling angle for varying entry angles ($\sigma_o = 0.025$ MPa; $\mu_{roll} = 0.35$).

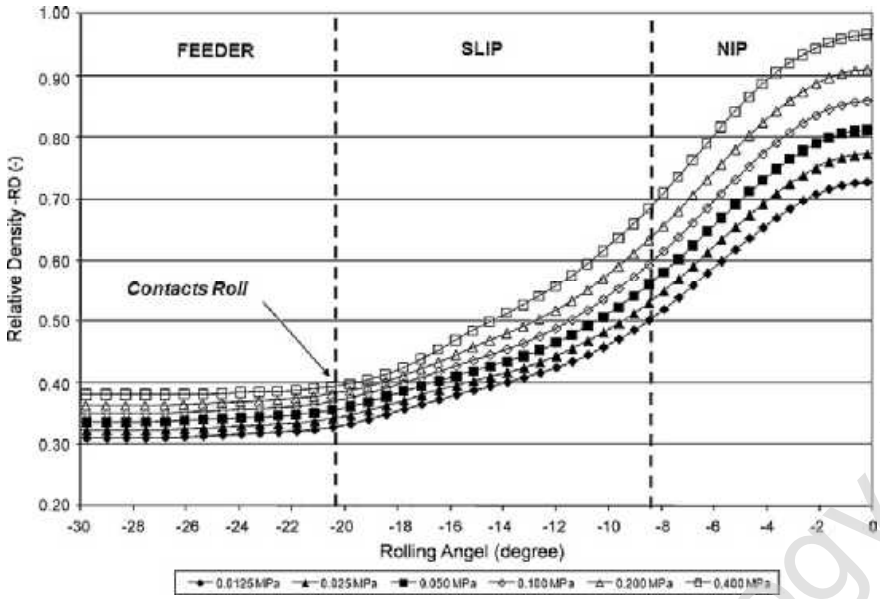

Fig. 12. Evolution of relative density with rolling angle for various feed stresses ($\alpha_{entry} = 20.5°$; $\mu_{roll} = 0.35$).

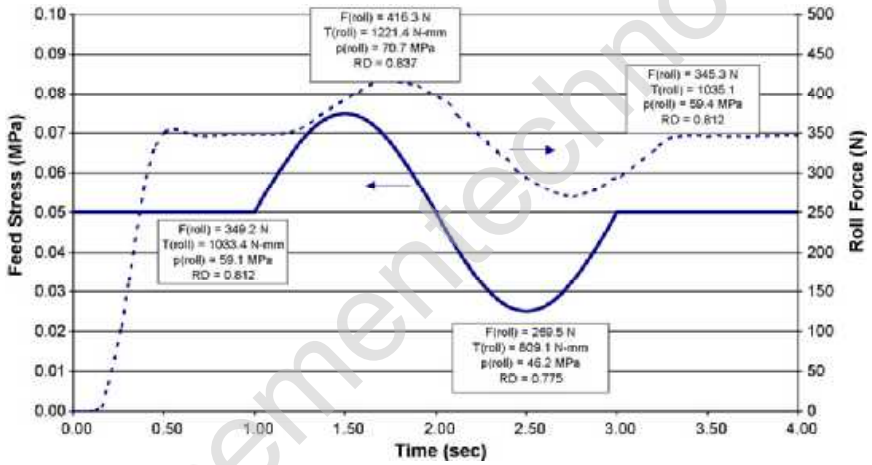

Fig. 13. The feed stress (prescribed) and resulting roll force as a function of time. The specific value of roll force, roll torque, maximum roll pressure and maximum relative density are shown ($\alpha_{entry} = 20°$, and $\mu_{roll} = 0.40$).

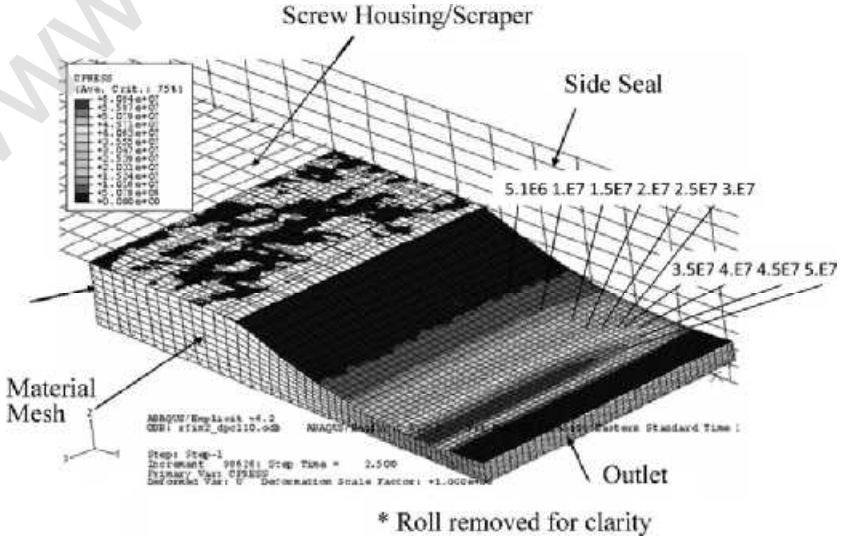

Fig. 14. Mesh, screw housing and side seal for 3D simulations. Roll was removed for clarity.

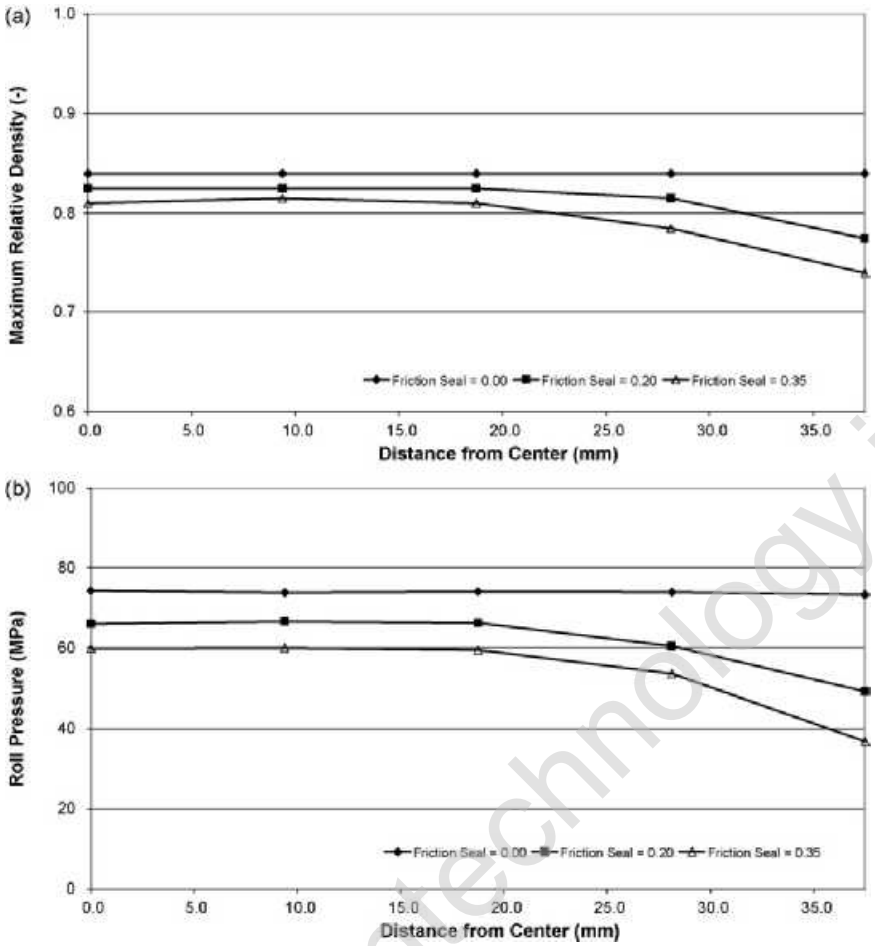

Fig. 15. (a) Maximum roll pressure along the transverse direction based on distance from the (b) maximum relative density along the transverse direction based on distance from the center (with 0 mm at the center and 37.5 mm at the side seal) for side seal friction of μ_{side_seal} = 0, 0.20 and 0.35.

the roll for higher friction and greater densification is obtained in the nip region with higher values roll pressure developed. As expected in a rolling process, the roll friction is a key parameter, although the results also indicate that there is a limit on the friction coefficient above which the effect of friction is limited.

In the case of powder compaction, it has been observed that the friction between the powder and the surface of the equipment may vary with the normal stress, relative density and/or relative velocity, e.g., in case of die compaction (Sinka et al., 2003). To assess the significance of varying μ_{roll}, a series of simulations in which μ_{roll} decreased from constant values following either a linear reduction or varying degrees of exponential reduction with the roll pressure as shown Fig. 10. The resulting relative density and maximum roll pressure can vary significantly. These results highlight the importance of appropriate definition of μ_{roll} under relevant conditions, e.g., normal stress, for modeling roller compaction. Although smooth rolls are sometimes used in roller compaction, often the roll has a textured surface that enhances the gripping action of the rolls. The contact conditions at the roll/powder interface in this case are more complex. Low pressure shear cell tests using coupon surfaces reflecting the surface properties can be useful for low stress states but higher normal stresses are usually prevail in roller compaction. In addition, in some cases the powder may adhere to a textured surface and friction is effectively shearing of a layer powder adjacent to the rolls. Although it was not attempted here, the use of finite element modeling with textured rolls has been conducted with briquetting (Zavaliangos, Dec, & Komarek, 2003). Given its importance in roller compaction, further assessment of the frictional properties of the textured surfaced is warranted.

4.3. Effect of entry angle

Profiles of relative density for varying entry angles are shown in Fig. 11 for the case of μ_{roll} = 0.35; σ_o = 0.025 MPa. The relative density achieved increased with increasing entry angle. The value of nip angle, i.e. approximately 8°, was unaffected by the entry angle in the range of 15–25°. In each case, the powder was predensified in the feed zone to the same degree due to the constant feed stress of 0.025 MPa. The powder continues to densify in the slipping region under the action of the roll friction and feed stress. Since the higher entry angle provided a longer slip region for densification to occur the powder reached higher level of densification prior to the nip angle. The densification in the nip region, is similar for all entry angles since the additional volume reduction is dictated by geometrical considerations between the nip angle and the centerline of the rolls, which are essentially the same for different entry angle studied.

4.4. Effect of feed stress

The effect of constant feed stress can be observed in the level of pre-densification in the feeder before the powder contacts the rolls (Fig. 12). Although the nip angle is not affected by the feed stress, higher feed stress increases the density of the powder in the feeder. The powder continues to densify under the rolls in

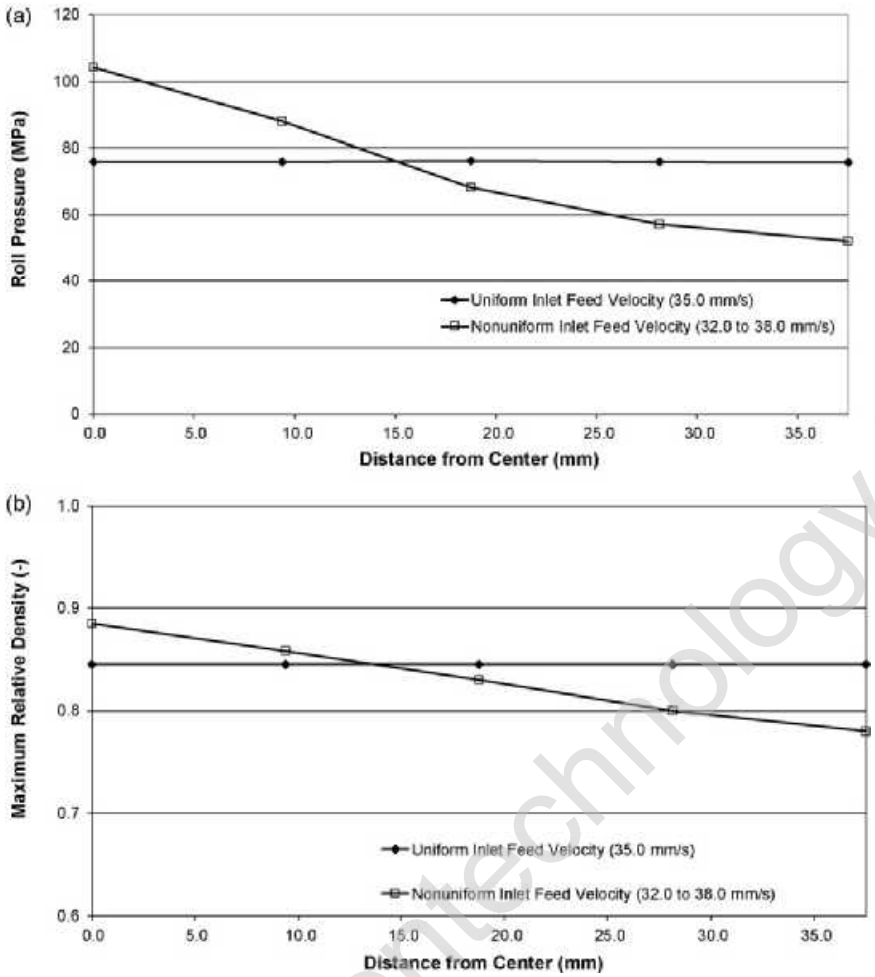

Fig. 16. (a) Maximum roll pressure along the transverse direction based on distance from the center. (b) Maximum roll pressure along the transverse direction based on distance from the center (with 0 mm at the center and 37.5 mm at the side seal) for uniform and non-uniform inlet velocity.

the slip region and consequently achieves higher final densification. Since the densification is the result of the feed stress higher entry angles require significantly higher feed forces to maintain a constant feed stress, e.g., the feed force must be increased by 48% and 110% to apply the same feed stress at entry angles of 20° and 25°, respectively, compared to 15°. Whether a specific roller compactor can achieve this level of feed force depends on the feeder design.

In practice, the screw feeder does not induce a constant feed stress but rather it is oscillatory in nature (Dec & Komarek, 1993). To simulate this effect feed stress was prescribed as a sinusoidal boundary condition for the case in which $\alpha_{entry} = 20°$, and $\mu_{roll} = 0.40$. The prescribed feed stress and resulting roll force, roll torque, the relative density at the exit, and the maximum pressure are provided at select time points in Fig. 13. Although there is a lag related to the movement of material already with the nip when feed stress changes, the parameters listed above follow corresponding sinusoidal fluctuations in values. The oscillatory nature of the feed stress is directly reflected in the other process parameters and compact properties.

5. Three-dimensional finite element model

The mesh representing the deforming powder was defined by a $20 \times 9 \times 54$ array using 3D continuum elements. We assume a four-fold symmetry which allows us to model only one quarter of the geometry. Fig. 14 provides the mesh and the key boundary information. The mechanical behavior of the powder was described using the Drucker-Prager/cap with the same material parameters used in the 2D model. The explicit formulation of ABAQUS with the arbitrary Lagrangian Eulerian (ALE) and adaptive meshing features were used to handle the non-linear contact conditions and severe distortion of the mesh due to the high shear conditions induced in rolling. Similar to the 2D model, Eulerian inflow and outflow boundaries were employed. The roll, seal side and screw housing were represented by rigid surfaces. The contact between the deformable mesh and these surfaces were defined by Coulomb's frictional law ($\mu_{screw} = 0$ on screw housing and variable on roll/powder and powder/side seal interfaces). For all the simulations above, the roll gap to roll diameter ratio was taken to be $2h_o/D = 0.02$ and the roll width to roll diameter $W/D = 0.375$, where W is the roll width. The entry angle was taken to be $\alpha_{entry} = 20°$. All the results presented correspond to steady state conditions.

5.1. Effect of side seal friction

Three simulations with the Coulomb coefficient of friction between powder and side seal $\mu_{side\_seal} = 0$, 0.2 and 0.35. In these simulations the feed stress was kept at 0.1 MPa. Fig. 15 shows the maximum roll pressure along the transverse (roll width) direction for the three frictional cases for the seal side. In the frictionless case, the maximum roll pressure is uniform across the transverse direction. As the side seal friction increased the roll pressure decreases

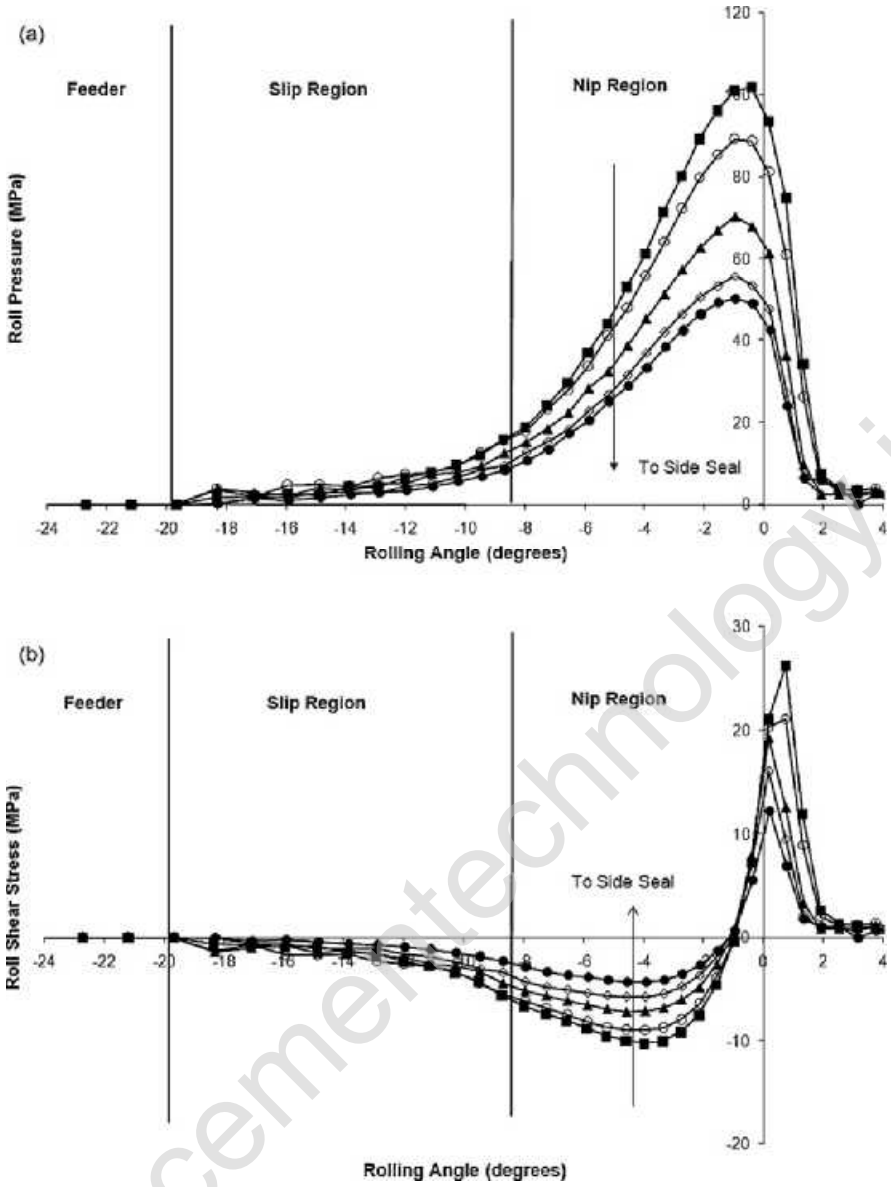

Fig. 17. (a) Profile of roll pressure versus rolling angle at various positions along the transverse direction from the center. (b) Profile of roll shear stress versus rolling angle at various positions along the transverse direction from the center.

as the side seal friction counteract the effect of the feed stress. The roll pressure also is reduced close to side seal with the highest side seal friction creating the largest reduction. The corresponding maximum relative density is plotted in Fig. 15. It is evident that increasing the side seal friction results in lower densification and greater variation in the transverse direction. To reduce adverse effect of friction, the side seals are typically manufactured with materials with low friction properties.

5.2. Effect of variable inlet velocity

Two simulations with constant (35 mm/s) and variable (32 mm/s at the sidewall to 38 mm/s at the center in a linear manner) inlet velocity to simulate the effect of non-uniform feeding due to the presence of the screw. The friction coefficient between powder and side seal was 0.35. In these simulations in which the side seal friction is zero and the inlet feed velocity is either uniform or linearly decreasing from the center to the edge. By adjusting the inlet velocity of the feed powder, the flux of powder entering rolls varies. This simulation is an attempt to understand aspects of inhomogeneity that may be associated with the presence and operation of the screw. In the case of uniform inlet velocity the maximum roll pressure and corresponding maximum relative density was the same along the transverse direction as shown in Fig. 16. Since there is no side seal friction, the uniform inlet velocity results in a uniform development of roll pressure. When the inlet velocity varies, i.e., the powder is preferentially fed to the center versus the edge, higher maximum roll pressures are developed toward center than the edge near the side seal. Fig. 17 provides the profiles of roll pressure and roll shear stresses across the roll width. The nip angle was the same across the roll but higher roll pressure and corresponding shear stresses developed in the center where material was preferentially fed, i.e., the high inlet velocity resulted in higher amount of material being fed to the center and consequently high density and roll pressures.

The results of these simulations indicate that both the side seal friction and the non-uniform feeding of the powder to the rolls may be contributing to the non-uniformity in roll pressure and density across the roll width. Lower densification at the edges has been attributed to the frictional resistance of the side seal to the flow

of powder. Improvements in the densification of the edges have been identified through 3D FEM simulation by in which the side seal rotated (Wang, Cunningham, & Zavaliangos, 2003). The screw feeder may also contribute to the non-uniformity across the transverse. The powder transitions from a circular cross-section related to the screw housing to a rectangular cross section associated with the rolls. The powder must re-distribute in this region of the feed zone. In addition, the oscillating screw is delivering material in a non-uniform manner across the roll width. These variations have been observed especially when the tip of the screw is very close to the nip where there is inadequate opportunity for the powder to rearrange. These variations are reflected in the maximum roll pressures generated and the density developed along the width. The screw feeder not only conveys the powder to the rolls but also generates a feed stress that varies depending on the screw relative position and the material distribution within the feed zone. The information on the spatial distribution of the material in terms of the relative density in the feed zone along with the feed force distribution in the feed zone are important initial and boundary conditions to be considered in understanding roller compaction in three dimensions.

6. Conclusions

The experimental studies using an instrumented roll to measure the local roll surface and roll shear stress provided valuable information on the degree of variation in the evolution of the contact stresses across the roll width and in the rolling direction and can allow stronger correlation to be developed with the observed spatial variations in the properties of the roller compacted material, e.g., relative density. The information from the instrumented roll also provided a deeper understand of the relationship to readily measurable process parameters like roll force. To gain great insight to these variations, 2D and 3D process modeling using the finite element method was conducted. A two-dimensional, plane strain continuum model of the roller compaction of pharmaceutical powders was developed that incorporated a pressure-dependent, frictional plasticity model, i.e., a modified DP/C model, to describe the stress–strain behavior of the powder over the range of relative densities experienced in the feed, slip and nip regions. To address the high shear conditions and accompanying deviatoric strains, an explicit formulation of the finite element method was used with adaptive meshing and Arbitary Eulerian Lagrangian (ALE) capabilities. The 2D simulations with roll pressure-dependent frictional coefficient indicated appreciable differences in development of roll pressure and densification of the powder depending on the functional relation between friction and the roll pressure. The oscillating feed stress conditions indicated anticipated periodic variations in maximum roll pressure and exit relative densities. Variations in the through-the-thickness were significant in the slip region and diminished as the powder moved through the nip region. The model predictions followed similar trends observed in the published experimental studies. The 3D results highlighted the variation in roll pressure in the roll width based on frictional properties of the side seal and variation in the feeding across the roll width. While additional refinement of the model will enhance its capabilities, e.g., more accurate experimental description of the friction conditions at the roll surface under relevant stress states and of the feed conditions (local relative density and feed stress), the current model provides a basis for greater understanding of the relative importance of various parameters, which can lead to more optimal design of experiments; improved equipment design, e.g., use of rotating side seal, and more effective interpretation of experimental data. With increasing capabilities of computational software and cross-fertilization of ideas and methodologies across disciplines and industries, the contributions of process modeling can be significant in the design, development and scale up of pharmaceutical processes.

Acknowledgements

The authors thank the technical contributions of Ed Roland of RRDI (instrumented roll and experimental studies), Jim Zega and Robert Meyer of Merck & Co. (experimental studies). In addition, the authors thanks Scott Reynolds of Merck & Co. for overall guidance and support of the modeling and experimental efforts. Funding for this work was provided by NSF-GOALI award CMS-0100063. The completion of this work was made possible by NSF-CMII-0900476.

References

Alkhattat, I. M., & Alhassani, S. T. S. (1987). Towards a computer-aided analysis and design of tablet compaction. *Chemical Engineering Science*, *42*(4), 707.
Andersen, K. T. (1990). Experimental measurements of pressure distributions in cement roller presses. In *9th international conference on experimental* Technical University of Denmark.
Bijlani, V., Anderson, C., Adeyeye, C., & Drennen, J. K. (2003). Near infrared spectroscopy for determining the hardness of roller compacted briquettes. *NIR News*, *14*(6), 7.
Bindhumadhavan, G., Seville, J. P. K., Adams, M. J., Greenwood, R. W., & Fitzpatrick, S. (2005). Roll compaction of a pharmaceutical excipient: Experimental validation of rolling theory for granular solids. *Chemical Engineering Science*, *60*, 3891.
Chekmarev, A. P., Klimenko, P. A., & Vinogradov, G. A. (1963). Investigation of specific pressure. Specific friction and the coefficient of friction during metal powder rolling. *Soviet Powder Metallurgy and Metal Ceramics*, 112.
Cunningham, J. C. (2005). *Experimental studies and modeling of roller compaction of pharmaceutical powders*. Philadelphia, PA: Drexel University.
Cunningham, J. C., & Zavaliangos, A. (2002). Experimental investigation and numerical simulation of roll compaction of powders. In Compiled by A. Lawley, J. E. Smugereski, L. Smith (Eds.), *Proceedings of the 2002 international conference on process modeling in powder metallurgy & particulate materials*. Newport Beach, California, USA, 28–29 October 2002; Metal Powder Industries Federation, Princeton, NJ, USA.
Cunningham, J. C., Sinka, I. C., & Zavaliangos, A. (2004). Analysis of tablet compaction. I. Characterization of mechanical behavior of powder and powder/tooling friction. *Journal of Pharmaceutical Sciences*, *93*(8).
Dec, R. T., & Komarek, R. K. (1991). Computer aided design of roll type briquetters and compactors. *Proceedings of the Institute for Briquetting and Agglomeration*, *22*, 1.
Dec, R. T., & Komarek, R. K. (1993). Testing performance of roll press force feed systems. *Proceedings of the Institute for Briquetting and Agglomeration*, *23*, 65.
Dec, R. T., Zavaliangos, A., & Cunningham, J. C. (2003). Comparison of various modeling methods for analysis of powder compaction in roller press. *Powder Technology*, *130*, 265.
Freitag, F., Reincke, K., Runge, J., Grellmann, W., & Kleinbudde, P. (2004). How do roll compaction/dry granulation affect the tableting behavior of inorganic materials? Microhardness of ribbons and mercury porosimetry measurements of tablets. *European Journal of Pharmaceutical Sciences*, *22*, 325.
Funakoshi, Y., Asogawa, T., & Satake, E. (1977). The use of a novel roller compactor with a concavo-convex roller pair to obtain uniform compacting pressure. *Drug Development and Industrial Pharmacy*, *3*(6), 555.
Guigon, P., & Simon, O. (2003). Roll press design—Influence of force feed systems on compaction. *Powder Technology*, *130*, 41.
Gun, G. Y., Stebunov, S. A., & Katashinskii, V. P. (1986). Computer modeling and investigation of the metal powder rolling process. *Poroshkovaya Metallurgiya*, *1*(277), 10.
Gupta, A., Peck, G. E., Miller, R. W., & Morris, K. R. (2004). Nondestructive measurements of the compact strength and the particle-size distribution after milling of roller compacted powders by near-infrared spectoscopy. *Journal of Pharmaceutical Sciences*, *93*(4), 1047.
Han, L. H., Elliott, J. A., Bentham, A. C., Mills, A., Amidon, G. E., & Hancock, B. C. (2008). A modified Drucker-Prager Cap model for die compaction simulation of pharmaceutical powders. *International Journal of Solids Structures*, *45*(10), 3088.
Herting, M. G., & Kleinebudde, P. (2007). Roll compaction/dry granulation: Effect of raw material particle size on granule and tablet properties. *International Journal of Pharmaceutical Sciences*, *338*, 110.
Hibbitt, Karlsson, & Sorensen. (2001). *ABAQUS manual version 6.2*. Pawtucket, RI: Hibbitt, Karlsson & Sorensen, Inc.
Johanson, J. R. (1965). A rolling theory for granular solids. *Journal of Applied Mechanics, Transactions of ASME*, *32*(4), 842.
Johanson, J. R. (1973). Predicting limiting roll speeds for briquetting presses. In *Proceedings of the 13th biennial conference* The International Briquetting Association, (p. 89).
Katashinskii, V. P. (1966). Analytical determination of specific pressure during the rolling of metal powders. *Poroshkovaya Metallurgiya*, *10*(46), 1.

Katashinskii, V. P., & Shtern, M. B. (1983a). Stress-strained state of powder being rolled in the densification zone. I. Mathematical model of rolling in the densification zone. *Poroshkovaya Metallurgiya*, *11*(251), 17.

Katashinskii, V. P., & Shtern, M. B. (1983b). Stress-strained state of powder being rolled in the densification zone. II Distribution of density, longitudinal strain and contact stress in the densification zone. *Poroshkovaya Metallurgiya*, *12*(252), 9.

Katashinskii, V. P., & Vinogradov, G. A. (1965). A Method of studying specific friction forces and pressures in the rolling of metal powders. *Poroshkovaya Metallurgiya*, *2*(26), 4.

Lecompte, T., Doremus, P., Thomas, G., Perier-Camby, L., LeThiesse, J.-C., Masteau, J.-C., et al. (2005). Dry granulation of organic powders—Dependence of pressure 2D distribution on different process parameters. *Chemical Science Engineering*, *60*, 3933–3940.

Lubjuhn, U., Sander, U., & Schonert, K. (1994). Pressure profile in the compression zone of the high-pressure roller mill. *Zement-Kalk-Gips (cement lime and gypsum) [english translation]*, *6*, E157.

Mansa, R. F., Bridson, R. H., Greenwood, R. W., Barker, H., & Seville, J. P. K. (2008). Using intelligent software to predict the effects of formulation and processing parameters on roller compaction. *Powder Technology*, *181*, 217.

Michrafy, A., Ringenbacher, D., & Tchoreloff, P. (2002). Modeling the compaction behavior of powders: Application to pharmaceutical powders. *Powder Technology*, *127*, 257.

Miguelez-Moran, A. M., Wu, C.-Y., Dong, H., & Seville, J. P. K. (2009). Characterisation of density distributions in roller-compacted ribbons using micro-indentation and X-ray micro-computed tomography. *European Journal of Pharmacy and Biopharmacy*, *72*, 173.

Musikhin, A. M. (1977). Deformation region stresses in the cold rolling of metal powders. *Poroshkovaya Metallurgiya*, *12*(180), 32.

Pietsch, W. (1987). *Roll pressing* (second ed.). London: Powder Advisory Center.

Procopio, A., Zavaliangos, A., & Cunningham, J. C. (2003). Analysis of the diametrical compression test and its applicability to plastically deforming materials. *Journal of Material Sciences*, *38*, 3629.

Schonert, K., & Sander, U. (2002). Shear stresses and material slip in high pressure roller mills. *Powder Technology*, *122*, 136.

Shima, S., & Yamada, M. (1984). Compaction of metal powder by rolling. *Powder Metallurgy*, *27*(1), 39.

Simon, O., & Guigon, P. (2000). Interaction between feeding and compaction during lactose compaction in a laboratory roll press. *KONA*, *18*, 131.

Simon, O., & Guigon, P. (2003). Correlation between powder packing properties and roll press compact heterogeneity. *Powder Technology*, *130*, 257.

Sinka, I. C., Cunningham, J. C., & Zavaliangos, A. (2003). The effect of wall friction in the compaction of pharmaceutical tablets with curved faces: A validation study of the Drucker-Prager Cap model. *Powder Technology*, *133*(1–3), 33.

Sinka, I. C., Cunningham, J. C., & Zavaliangos, A. (2004). Analysis of tablet compaction. II—Finite element analysis of density distributions in convex tablets. *Journal of Pharmaceutical Sciences*, *93*(8), 2040.

Tunderman, J. H., & Singer, A. R. E. (1969). Deformation and densification during the rolling of metal powder. *Powder Metallurgy*, *12*, 219.

Wang, W., Cunningham, J. C., & Zavaliangos, A. (2003). The effect of side constraint in rolling compaction of powder. In *International conference on powder metallurgy & particulate materials* Las Vegas, Nevada.

Weyenberg, W., Vermeire, A., Vandervoort, J., Remon, J. P., & Ludwig, A. (2005). Effects of roller compaction on the preparation of bioadhesive granules and ocular minitablets. *European Journal of Pharmacy and Biopharmacy*, *59*, 527.

Wu, C. Y., Ruddy, O. M., Bentham, A. C., Hancock, B. C., Best, S. M., & Elliott, J. A. (2005). Modelling the mechanical behaviour of pharmaceutical powders during compaction. *Powder Technology*, *152*(1–3), 107.

Zavaliangos, A., Dec, R. T., & Komarek, R. K. (2003). Analysis of powder processing in the roller press using finite element modeling. In *XXII international mineral processing congress* Cape Town, S. Africa.

Zavaliangos, A., Galen, S., Cunningham, J., & Winstead, D. (2008). Temperature evolution during compaction of pharmaceutical powders. *Journal of Pharmaceutical Sciences*, *97*(8), p3291.

Zega, J., Cunningham, J., Roland, E., Katdare, A., & Reynolds, S. (1998). Experimental investigation of the fundamental parameters of roller compaction. In *1998 AAPS annual meeting* San Francisco, CA.